Inferring the Dielectric Properties of Oil Slick from Multifrequency SAR imagery via a Polarimetric Two-Scale Model

Cornelius P. Quigley, Camilla Brekke, Torbjørn Eltoft
UiT The Arctic University of Norway, Tromsø, Norway.

Abstract

We apply a polarimetric two-scale model to multifrequency synthetic aperture radar imagery of verified oil slicks measured by DLRs F-SAR instrument, which can acquire high spatial resolution and high signal-to-noise data. The purpose, is to determine the permittivity of the scattering surface via an inversion procedure. The ocean surface is modelled as an ensemble of randomly orientated, tilted facets for which the small perturbation model is assumed valid under the condition of no tilt. Only co-polarization channels are utilized due to system noise, hampering the signal within the cross-polarization channels. Results yield realistic results for the permittivity of oil slick.

1 Introduction

Mineral oils, that are present in the marine environment, are easily detectible by Synthetic Aperture Radar (SAR) sensors as they appear as dark patches. These surface slicks reduce the backscatter to the SAR via two physical mechanisms. The first, is that they dampen the short-scale, wind induced capillary waves, which reduces the short-scale roughness of the ocean surface, resulting in a reduction of backscatter to the sensor, see, e.g., [1]. This reduction in backscatter necessitates the use of sensors that can provide a reasonable signal-to-noise ratio (SNR) for the determination of the dielectric properties of oil slick.

The second mechanism is directly related to the processes mineral oil undergoes when it is included into the marine environment which are collectively referred to as weathering [2]. One such process is emulsification, whereby the surface slick becomes thicker as sea water becomes entrained within it, which has the effect of reducing the effective dielectric constant of the ocean surface. These water-in-oil mixtures can result in a reduction of backscatter to the radar if the oil is mixed in high enough concentrations within a thin layer below the ocean surface [3].

Via the application of theoretical scattering models, it should be possible to invert the backscatter to retrieve estimated values of $|\varepsilon|$, the absolute value of the effective dielectric constant of the water-oil mixture. The evaluated dielectric value is fed into a mixing model which is inverted to determine the volumetric content of oil in a pixel, or the inverted dielectric values can be used to provide a heuristic based indication on where there are greater amounts of oil within slick compared to other areas.

In this study, a Polarimetric Two-Scale Model (PTSM) that is described in [4] is used to invert the co-polarimetric ratio for the absolute value of the complex permittivity $|\varepsilon|$. The model is applied to data acquired by Deutsches Zentrum für Luft- und Raumfahrt (DLR) F-SAR instrument in X-, S- and L-bands acquired simultaneously during the NOrwegian Radar oil Spill Experiment in 2019 (NORSE 2019) led by the Centre for Integrated Remote Sensing and Forecasting for Arctic Operations (CIRFA) as an embedded part of the Norwegian Clean Seas Association for Operating Companies (NOFO) annual oil-on-water campaign. This campaign took place in the North Sea in June 2019. F-SAR, being an airborne instrument, has the capability to acquire data with a low level of noise corruption, resulting in data sets with high signal-to-noise ratios (SNR).

In this study, simultaneous S and L-band imagery of a mineral oil emulsion slick were inverted for $|\varepsilon|$. While the estimated $|\varepsilon|$ values within the oil seem to be slightly underestimated for areas that correspond to the darkest parts of the slick in intensity values, they are not significantly different from the actual value of 2.3 [5]. The following sections will recap the theoretical aspects of our methodology, briefly outline the data set that is presented here and show results derived from the applied model.

2 Basic Method

2.1 Polarimetric Two-Scale Model

The Normalized Radar Cross Section (NRCS) return from a single tilted facet is defined as

$$\sigma^0_{HH} = \frac{4}{\pi}k^4 cos^4 v_l s^2 W_n(2ksin\, v_l) \times |F_H(v_l)cos^2\beta + F_V(v_l)sin^2\beta|^2$$
$$\sigma^0_{VV} = \frac{4}{\pi}k^4 cos^4 v_l s^2 W_n(2ksin\, v_l) \times |F_V(v_l)cos^2\beta + F_H(v_l)sin^2\beta|^2 \quad (1)$$

v_l is the local incidence angle due to the facet tilt, β is the out-of-plane tilt of the tilted facets, k is the wavenumber of the incoming radiation, W_n is the power spectral density whose expression can be found in [4]. Expressions for the Bragg coefficients, F_H and F_V, whos form depends on ε, the complex permittivity of the scattering surface can also be found in [4]. In the PTSM, the NRCS within a single resolution are defined as

$$\langle\sigma^0_{HH}\rangle_{a,b} = \frac{4}{\pi}\left[C^{HH}_{0,0} + \left[C^{HH}_{2,0} + 2\frac{Re\{C^{HV}_{0,0}\} - C^{HH}_{0,0}}{sin^2 v} + C^{HH}_{0,2}\right]s^2\right]$$
$$\langle\sigma^0_{VV}\rangle_{a,b} = \frac{4}{\pi}\left[C^{VV}_{0,0} + \left[C^{VV}_{2,0} + 2\frac{Re\{C^{HV}_{0,0}\} - C^{VV}_{0,0}}{sin^2 v} + C^{VV}_{0,2}\right]s^2\right] \quad (2)$$

where s^2 is the variance of the slopes of the tilted facets, who's distributions are assumed to be Gaussian with zero mean, and is a measure of the large-scale roughness. Here, the terms $C_{k,n-k}^{pq}$ are the series expansion coefficients of the function $(k\ cos\ v_l)^4 W F_p F_q^*$ and can be found in [4]. The full expressions for $C_{0,0}^{pq}$, $C_{2,0}^{pq}$ and $C_{0,2}^{pq}$ were derived numerically. The superscripts p and q indicate the send and receive polarizations respectively. $\langle \sigma_{pq}^0 \rangle_{a,b}$ denotes ensemble averaging of the NRCS from a single tilted facet over the slopes of the facet in range and azimuth i.e. a and b respectively.

2.2 Inversion Procedure

The co-polarization ratio for the NRCS is defined as

$$Co-pol = \frac{\langle \sigma_{VV}^0 \rangle_{a,b}}{\langle \sigma_{HH}^0 \rangle_{a,b}}. \quad (3)$$

The benefit of using the polarization ratios is that the dependence on the small-scale roughness is removed and we are left with an equation that depends on |ε| and *s*. In order to estimate *s* without the use of the cross-polarization channels, the following method was employed.

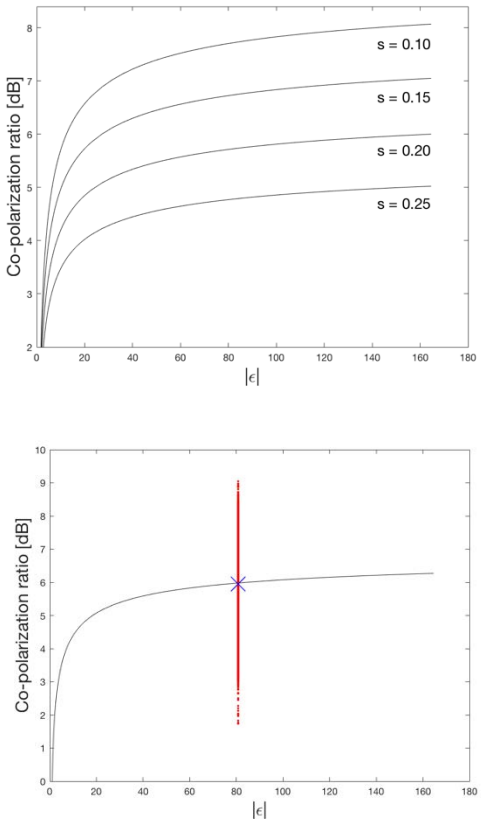

Figure 1: (Above) PTSM co-polarization curves, computed for various values of s, in S-band, with an incidence angle of 47°. (Below) Method for estimating s. The red line is scatter taken from a portion of the co-polarization ratio, as defined in (1), over clean ocean. The blue X is the mean of the scatter. The s value for which the PTSM curve coincides with X at the dielectric value for water is used, and is assumed a valid estimation for s.

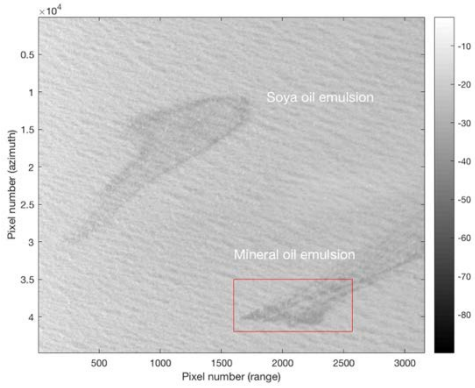

Figure 2: Intensity image (σ_{0VV} [dB]) in S-band acquisition, multi-looked by 9x9 window. The region-of-interest of the slick of emulsion is outlined with a red box. FSAR data provided by DLR - Microwaves and Radar Institute.

It can be seen in Figure 1 that the model is heavily dependent on the value of *s*. The regions containing slicks were manually masked out, then the entire scene was divided into square regions of size 100x100 pixels. The scatter of co-polarization values from each square region was plotted at a value of |ε| that corresponds to open water in the North Sea under the given conditions (temperature and salinity). The value of *s* that corresponds to the average of the co-polarization scatter, seen as a blue X in Figure 1, was taken as an estimate for *s*. It is believed that the large-scale roughness is similar across open water and oil slick, so the values for *s* within slick, were estimated from the values that were found for the surrounding open, ocean immediately adjacent to the slick.

3 Data set and Inversion Results

In this paper, we apply the PTSM to data acquired during the NORSE 2019 oil-on-water campaign conducted in the North Sea (N 59° 59', E 2° 27'). Figure 2 shows the S-band FSAR acquisition of the two verified slicks that were discharged during the campaign. One was 2 m^3 of soya oil, which was used to simulate natural monomolecular biogenic slicks, the other was 2 m^3 of crude oil emulsion. Table 1 summarizes the relevant information pertinent to the acquisition as well as wind conditions present.

Figure 3 shows the inversion results for the slick of emulsion that is highlighted in Figure 2, as well as the damping ratios in both S- and L-bands. The damping ratio refers to the ratio of clean sea pixels to oil slick pixels in the VV polarimetric channel. While the model was originally allowed to run to the arbitrary high value of |ε| equalling 165, in the results presented in Figure 3, an upper bound 60 was imposed. This was to create a framework in which to compare the two inversion results. Since |ε| values for oil infested areas are expected to be significantly lower, i.e. below 30 approximately, this does not affect the results significantly. The damping ratio images were also truncated to between values of 2 and 20 for the sake of comparison

Table 1: Properties of SAR acquisition

Date	12 June 2019
Incidence angle (of emulsion slick)	51° - 57°
Resolution (Rg x Az) [m]$_{(X-,S-,L-Band)}$	(0.3 x 0.2) (0.75 x 0.35) (1.5 x 0.4)
Wind speed	12 m/s

It should be noted that the surrounding ocean areas were masked out before the inversion procedure was implemented and that the mask was drawn by hand.

As expected, the inversion results of the L-band data yield significantly higher values for $|\varepsilon|$ than the S-band results. This is due to the higher wavelength of the L-band acquisition, which was acquired with a wavelength of 22.6 cm as opposed to 9.2 cm for the S-band acquisition. Oil that is too thin on the scale of the wavelength of the incoming radiation will not contribute to the backscatter to the sensor. For the case of L-band, this means that there is a higher probability of the backscattered radiation being reflected at the ocean surface, rather than interacting with the overlying slick, if the slick layer is thin enough.

The damping ratio for the two acquisitions is also included as a reference as it is believed that the damping ratio can serve as a proxy for the oil thickness [6] and it gives an indication of the relative thickness distribution within slick. When comparing the inverted $|\varepsilon|$ results to the corresponding damping ratio imagery certain corresponding areas between the two can be observed. The most prominent of these is a thin long strip, running the length of the slick. Examining Figure 2 it is believed that this corresponds to an area within the slick where there is a low amount of oil present. In the inversion results for both L- and S-band this corresponds to high values of $|\varepsilon|$ while in the damping ratio imagery for both L- and S-band, this long strip can be seen to have low values. Both these results are consistent with a low presence of oil. This effect can also be seen when comparing the $|\varepsilon|$ results at the head of the slick for S-band in Figure 3, middle panel, left, and the corresponding damping ratio in Figure 3, middle panel, right. In the $|\varepsilon|$ imagery, this area has high values for $|\varepsilon|$ while in the damping ratio image there are low values across the head of the slick.

It is also interesting to note that when comparing the damping results between L- and S-band, there seems to be a higher degree of damping of backscatter in the S-band imagery when compared to L-band. This is most likely due to the higher likelihood of the S-band radiation being damped more due to its shorter wavelength compared to L-band.

Figure 3, bottom panel left, shows the difference between the L-band $|\varepsilon|$ values and the S-band $|\varepsilon|$ values in the form of $L_{|\varepsilon|} - S_{|\varepsilon|}$. As expected, a large portion of this image has high values indicating the areas that were observed to have $|\varepsilon|$ values closer to that of water in the L-band acquisition but to have $|\varepsilon|$ values closer to that of oil in the S-band acquisition (yellow pixels). Inversely, the areas that were observed to have $|\varepsilon|$ values close to that of oil in the L-band inversion but closer to that water in the S-band acquisition are less numerous, but can still be observed (dark blue pixels). This is somewhat counterintuitive as it is expected that if the sensor indicates an area of oil in L-band it should be correspondingly indicated within the S-band inversion results. It is not sure what the reason for this discrepancy arises but may be related to the higher level of noise in the S-band acquisition as compared to the L-band acquisition. Areas where there were more correspondence between the two can be observed as having values closer to zero (green pixels).

Figure 3, bottom panel, right, shows the absolute value of the difference between inversion results i.e. $\left|L_{|\varepsilon|} - S_{|\varepsilon|}\right|$. Internal zones, which are believed to contain the most oil are highlighted. This image is similar in appearance to the $|\varepsilon|$ inversion results from the L-band acquisition. This is expected as the L-band radiation would only be modified by the thicker parts of the slick as a thicker slick is expected to dampen the longer ocean waves which are responsible for the L-band backscatter

4 Conclusions and Future Work

This work presents results of the application of the PTSM for the estimation of $|\varepsilon|$ to SAR imagery of ocean dwelling surface slicks. The work extends the original PTSM in that a procedure to estimate the large-scale roughness of the ocean surface from the co-polarization ratio is developed and incorporated. This is necessary as the model has two primary unknowns that can be easily inverted if cross-polarization data is available.

Future work will focus on verifying the use of the PTSM via use of the co-polarization imagery by testing the procedure with the cross-polarization ratio incorporated. Given the low noise floor of the FSAR instrument it is believed this will yield significant results.

Acknowledgment: We would like to thank CIRFA (RCN project number 237906), Total E&P Norge AS, NOFO for allowing our participation in OPV2019, DLR and the F-SAR crew for collaborating on data collection during NORSE2019.

Literature

[1] B. Minchew, C. E. Jones, B. Holt. Polarimetric analysis of backscatter from the Deepwater Horizon oil spill using L-band synthetic aperture radar. *IEEE TGRS* vol. 50, no. 10, pp. 3812-3830, Oct. 2012.

[2] J. Coleman, Ed. *Oil in the Sea III: Inputs, Fates and Effects*. The National Academic Press, 2003.

[3] S. Angelliaume, O. Boisot, C.A. Guerin. Dual-Polarized L-Band SAR Imagery for Temporal Monitoring of Marine Oil Slick Concentration. *Remote Sens.,* vol. 10, no. 7, Jul. 2018.

[4] A. Iodice, A. Natale, D. Riccio. Retrieval of soil surface parameters via a polarimetric two-scale model. *IEEE TGRS* vol. 49, no. 7, pp. 2531-2547, Jul. 2011.

[5] K. Folger. Bilinear caliration of coaxial transmission/reflection cells for permittivity measurements of low-loss liquids. *Meas. Sci.Technol.,* vol. 7, no. 9, pp-1260-1269, Sept. 1996.

[6] S. Skrunes, C. Brekke, and M. M. Espeseth. Assessment of the RISAT-1 FRS-2 mode for oil spill observation. IEEE (IGARSS), pp. 1024–1027, 201

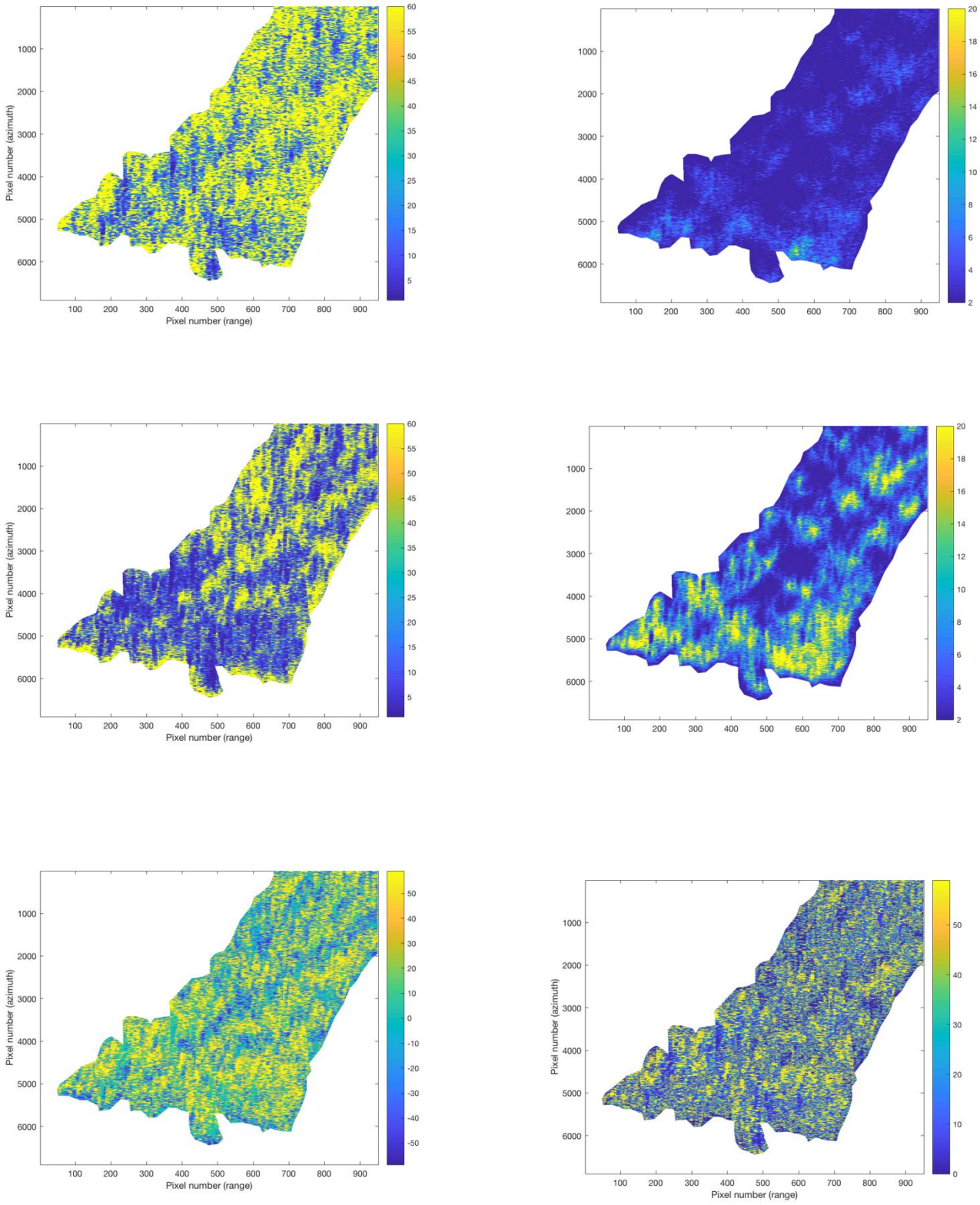

Figure 3: Top panel left, the inversion results of $|\varepsilon|$ for the slick of emulsion in L-band. Top panel right, damping ratio derived from the VV L-band channel. Middle panel left, the inversion results of $|\varepsilon|$ for the slick of emulsion in S-band. Middle panel right, damping ratio derived from the VV S-band channel. Bottom panel left, difference between inverted $|\varepsilon|$ values derived from both L- and S-band i.e. $|\varepsilon|$ derived from L-band minus $|\varepsilon|$ derived from S-band. Bottom panel right, absolute value difference between inverted $|\varepsilon|$ values derived from both L- and S-band.